Ordering of alkali halide salts dissolved in bacteriophage Pf1 solutions: A nuclear magnetic resonance study

S. Vyas, C. J. Hernandez, and M. P. Augustine[a)]
Department of Chemistry, University of California, Davis, California 95616

(Received 4 October 2001; accepted 30 January 2002)

The nuclear magnetic resonance (NMR) spectra of the $I=3/2$ monovalent ions ^{23}Na, ^{35}Cl, ^{39}K, and ^{79}Br for NaCl and KBr dissolved into filamentous bacteriophage Pf1 solutions display line splittings and shifts consistent with an interaction between the nuclear spin and the electric field gradient produced by the Pf1 particles. The average electric field gradient and thus the spectral splitting for ions in the void space between magnetically aligned Pf1 particles is modeled using a numerical solution to the Poisson–Boltzmann equation. An NMR titration experiment in a 57 mg/mL Pf1 solution is used to determine the background Na^+ ion concentration in solution as 32 mM which compares well with the 31.1 mM negative surface charge on Pf1. © *2002 American Institute of Physics.* [DOI: 10.1063/1.1463396]

I. INTRODUCTION

The determination of chemical structure is a necessary first step towards understanding the properties of materials on a molecular scale. Nuclear magnetic resonance (NMR) spectroscopy is one example of many extremely powerful tools that have been widely used to determine three-dimensional molecular structure in solids, liquids, and gases. In the special case of biological liquid state NMR spectroscopy, it has been recently shown that the ordering of protein and nucleic acid solutes by collisions with large magnetically aligned constructs like phospholipid bicelles[1] and filamentous virus[2] and bacteriophage[3] particles partially restores anisotropic information to a high-resolution NMR spectrum. Two nice features of this approach are that the concentration of the aligned liquid crystalline medium is typically below the NMR detection threshold and that the residual couplings are introduced as spectral line splittings or scaled first order effects, instead of the typical second order change in line width or intensity.[4]

Residual spectral effects due to the chemical shift anisotropy and the spin–spin dipolar coupling for $I=1/2$ nuclei and the quadrupolar coupling for $I=1$ nuclei have been observed in filamentous bacteriophage media.[3] In the case of both aspherical macromolecular systems[1–3] and small aspherical molecules like D_2O[3] in aqueous phase, it is reasonable to assume a collisional model for the recovery of anisotropic information. Indeed, this alignment model is consistent with the literature involving the alignment of aspherical organic molecules dissolved in organic liquid crystalline media.[5] In the special case of solute molecules having no dipole moment but with D_{nh} symmetry like H_2 or C_6H_6, the interaction of the solute molecular quadrupole moment with the electric field gradient of the liquid crystalline medium is an important solute alignment mechanism.[6] The success of this solute alignment approach is of course predicated upon establishing a well defined electric field and corresponding field gradient between the molecules that comprise the liquid crystal. Liquid crystalline electric fields can be calculated by considering analogous physical problems. For example, the field in the void space between solvent molecules in an aqueous phase lamellar liquid crystal can be modeled in one dimension by considering a capacitor with equally charged plates and asking how the electric field varies from plate-to-plate when a dielectric solute like water is held between the plates.[7] Although successful in the description of the recovery of residual anisotropic effects in the NMR spectra of aspherical molecules, an interaction of the liquid crystal electric field gradient with the solute molecular quadrupole moment does not explain alignment effects in spherical molecular systems.[8] Here the tetrahedral structure of molecules like CH_4[8] and ND_4^+ (Ref. 9) is modified by the liquid crystalline medium, thus providing an axis of preferential alignment. This second-order effect is loosely equivalent to considering the interaction of the solute molecular electric polarizability with the electric field of the solvent. This model, however, breaks down in the case of simple monovalent ions like the alkali metals and the halides in solution. Here, the polarizability of the cations and anions is too small to account for the experimental observations.[10] Another approach typically assumes a two-site chemical exchange between ions bound to a polyelectrolyte and those free in solution.[11] Although exchange rates and coupling constants can be found that fit this model to experiment, the site-to-site coupling constant variability in real macromolecular systems suggests that this model is limited.

Reasonable agreement between experiment and theory for the residual spectral splitting of quadrupole ions dissolved in lamellar liquid crystal solvents has also been calculated directly from the electric field gradient produced by the lamellae. Here the average gradient was calculated by considering the ion distribution in real space.[12] A similar agreement between experiment and theory was also found by asserting that the charged lamellae perturb solvent molecular structure near the ion thus establishing a point charge or

a)Electronic mail: augustin@chem.ucdavis.edu

dipole potential at the nuclear spin.[13] The analytical form for the field gradient in these cases was used to describe the observable residual quadrupolar coupling in aqueous phase. In both of these examples, the effect of valence electrons around the nucleus in question was accounted for by incorporating the Sternheimer antishielding factor $1-\gamma_\infty$.[14] This parameter combined with a geometric correction due to the polarization of the medium by the charge defect was used to relate the external macroscopic field gradient to the internal field gradient experienced by the nuclear spin.[15]

Since these studies demonstrate that residual quadrupolar couplings can be recovered in spherical atomic ions using aqueous phase lamellar liquid crystals, an interesting question is whether or not these effects persist into the nematic phase. Here, molecules like the filamentous bacteriophages locally pack into well ordered arrays or domains. A partial answer to this question was provided by Van der Klink *et al.*[16] who investigated changes in ^{23}Na NMR relaxation times—second-order effects—due to ordered poly(acrylic acid). In this approach the time averaged mean-square field gradient was calculated using an analytical solution to the Poisson–Boltzmann equation provided by Fuoss *et al.*[17] The boundary conditions appropriate for this solution rely on taking the polyelectrolyte as having a negative surface charge and being infinitely long with a well defined mean distance between polyelectrolyte molecules. Half of this distance is used to assign a maximum in the electric potential, or the boundary for a single macromolecular volume or cell. Although successful in describing spin lattice T_1 and spin–spin T_2 relaxation effects in ^{23}Na, no residual first order effects such as quadrupolar splittings were reported.

A good system to study the recovery of first order quadrupole effects due to the potential of the polyelectrolyte rod is the filamentous bacteriophage Pf1, given the success of this system in the collisional recovery of residual dipolar couplings in proteins and nucleic acids and quadrupolar couplings in D_2O. Pseudomonas phage Pf1[18] is a simple rod-like molecule $\approx \ell = 2\ \mu$m long, $2a = 6.6$ nm in diameter, and with a molecular weight of 35 MD. The phage consists of a single stranded circular DNA molecule packed in a sheath of 7620 identical protein subunits. These coat protein subunits consist of 46 amino acids arranged in an α-helical structure that pack around the DNA and essentially maximize the magnetic susceptibility of the Pf1 molecule. The surface charge of the Pf1 molecule was explored by titration analysis revealing that there are 19 100 positive ion binding sites on the surface of the rod. This number can be used along with the 41 500 nm^2 surface area of Pf1 to calculate the surface charge density of 7.4 μC/cm^2, a number comparable to the charge density of a metallic electrode. These structural details suggest that it is safe to consider a Pf1 molecule as an infinitely long uniformly charged negative rod from the perspective of the $\approx$0.1 nm diameter atomic ions examined here.

With regards to earlier work in lamellar systems,[12] one expects that the electric field gradient will decrease as a function of displacement from the rod surface. Combining this expectation with the fact that positive ions will condense around the negative rod in a high electric field gradient region and that negative ions will be repelled from the rods into the region of low gradient between rods, suggests that the residual quadrupolar couplings for cations will be larger than for anions. It is the purpose of this paper to explore this expectation both experimentally and theoretically in Pf1 solution. The next section first provides a brief review of the NMR of $I>1/2$ nuclei in ordered media. It is shown in this section that the important parameter that can be used to compare experiment with theory is the average field gradient for positive + and negative − ions. This average gradient is calculated using a cell model that involves a solution to the Poisson–Boltzmann equation in cylindrical coordinates—a solution that naturally allows for both positive and negative free ions. This model is compared to experimental results for NaCl and KBr dissolved into different Pf1 solutions.

II. NMR SPECTRA OF ORDERED IONS

The Hamiltonian appropriate for the calculation of the energy of an isolated $I>1/2$ nuclear spin in an electric field gradient and a large static magnetic-field B_0 can be written to first-order in the rotating frame as

$$\mathcal{H}=\beta_Q\langle A_0^{(2)}\rangle T_0^{(2)}, \tag{1}$$

where $\beta_Q = eQ/2I(2I-1)h$, e is the electron charge, Q is the quadrupole moment of the spin I, and h is Planck's constant. The irreducible component of this Hamiltonian appropriate for the spin operators is given by

$$T_0^{(2)}=\frac{1}{\sqrt{6}}(3I_z{}^2-\boldsymbol{I}^2), \tag{2}$$

and the real space average in terms of the Wigner rotation matrix element $D_{q,0}^{(2)}(\alpha,\beta,\gamma)$ is

$$\langle A_0^{(2)}\rangle=\sum_q \langle D_{q,0}^{(2)}(\alpha,\beta,\gamma)R_q^{(2)}(r,\gamma)\rangle, \tag{3}$$

where the α, β, and γ Euler angles relate the elements of the electric field gradient tensor expressed in the rotating frame to the frame defined by the long axis of a Pf1 particle. The choice of a particle-based coordinate system is reasonable because the electric potential at the nucleus $V(r)$ is related to the source of the macroscopic electric potential, here the potential $V_r(r)$ produced by the charged rod. The three orders of magnitude difference in length scale between rod size and ion diameter prompts the approximation of the nematic phase of Pf1 used in this study as a collection of regularly spaced infinitely long charged cylinders. Therefore both $V_r(r)$ and $V(r)$ have cylindrical symmetry, only depend on the distance r from the Pf1 surface, and are related by the Sternheimer anti-shielding factor $1-\gamma_\infty$ as

$$V(r)=(1-\gamma_\infty)V_r(r). \tag{4}$$

The polarization correction factor $(2\varepsilon+3\varepsilon_0)/5\varepsilon$ where ε_0 is the vacuum permittivity and ε is the permittivity of the medium is intentionally not included in Eq. (4) because the potential $V_r(r)$ is not due to a single charge defect as is appropriate for ionic crystals.[15] This also implies that the values of the Sternheimer antishielding factors that have been computed for charge defects in ionic crystals[19–21] are

most likely not applicable in fluid phase. This inequivalence does not change the symmetry relationship between $V(r)$ and $V_r(r)$. Indeed, the cylindrical symmetry of $V(r)$ allows the irreducible components of the field gradient tensor in the Pf1 frame to be written as

$$R_0^{(2)}(r) = -\frac{1}{\sqrt{6}}\left(\frac{\partial^2}{\partial r^2} + \frac{1}{r}\frac{\partial}{\partial r}\right)V(r),$$
$$R_{\pm 2}^{(2)}(r) = \frac{1}{2}e^{\pm 2i\gamma}\left(\frac{\partial^2}{\partial r^2} - \frac{1}{r}\frac{\partial}{\partial r}\right)V(r), \tag{5}$$

where $R_{\pm 1}^{(2)}(r)$ is zero since $V(r)$ is independent of both the displacement z and the angle γ. The average in Eq. (3) reflects a statistical distribution of the values for α, β, γ, and r at any point in time. In the case of a magnetically aligned Pf1 nematic phase characterized by a magnetic susceptibility tensor χ, this average is different for positive and negative ions via a dependence on charge density as

$$\langle A_0^{(2)}\rangle_{\pm} = \sum_{q=-2}^{+2}\langle D_{q,0}^{(2)}(\alpha,\beta,\gamma)R_q^{(2)}(r)\rangle_{\pm}$$
$$= \sum_{q=-2}^{+2}\frac{\int e^{iq\alpha}d_{q,0}^{(2)}(\beta)P(\beta)\sin\beta d\alpha d\beta}{\int P(\beta)\sin\beta d\alpha d\beta}$$
$$\times\frac{\int R_q^{(2)}(r)\rho_{\pm}(r)rdrd\gamma}{\int\rho_{\pm}(r)rdrd\gamma}, \tag{6}$$

where the definition of $D_{q,0}^{(2)}(\alpha,\beta,\gamma)$ in terms of the Wigner reduced rotation matrix element $d_{q,0}^{(2)}(\beta)$ is used. The cylindrical symmetry of the Pf1 particle imparts axial symmetry on the susceptibility tensor which when combined with Boltzmann statistics can be used to assign the alignment probability $P(\beta)$ as $\ln[P(\beta)] = -\mathbf{B}\cdot\chi\cdot\mathbf{B}/kT$ where $\mathbf{B}$ is the applied static magnetic field, k is Boltzmann's constant, and T is temperature. The ion density can be likewise defined as $\ln[\rho_{\pm}(r)/eN_{\pm}] = \mp eV_r(r)/kT$ where $N_{\pm}$ is the positive or negative ion number density. In the usual limit when $\|\mathbf{B}\cdot\chi\cdot\mathbf{B}\| \gg kT$, the integral over $\sin\beta d\beta$ in Eq. (6) reduces to just the $q=0$ term because the probability $P(\beta)$ collapses to a delta function concentrated on the $+z$ axis parallel to B_0. The cylindrical symmetry of the potential $V_r(r)$ implies that the density $\rho_{\pm}(r)$ is independent of the angle γ. This also forces all terms with $q\neq 0$ in the integral over the $R_q^{(2)}(r)$ terms in Eq. (6) to zero. Therefore, the average in Eq. (6) reduces to

$$\langle A_0^{(2)}\rangle_{\pm} = \frac{\int R_0^{(2)}(r)\rho_{\pm}(r)rdr}{\int\rho_{\pm}(r)rdr} = \langle R_0^{(2)}\rangle_{\pm}, \tag{7}$$

which can be used along with Eqs. (1) and (2) to yield the Hamiltonian corresponding to the residual quadrupolar splitting for $I>1/2$ ions in Pf1 solution as

$$\mathcal{H} = \nu_Q(3I_z^2 - \boldsymbol{I}^2), \tag{8}$$

where the definition $\nu_Q = \beta_Q\langle R_0^{(2)}\rangle_{\pm}/\sqrt{6}$ is used.

Equation (8) can be used to determine the NMR spectrum for an $I>1/2$ nucleus in the liquid phase. In the specific case of an $I=3/2$ nucleus there are three $\Delta m = \pm 1$ transitions with intensity given by the square of the off diagonal matrix elements of the observable operator I_x. These matrix elements between angular momentum states $|m\rangle$ and $|m'\rangle$, where for $I=3/2$ $|m\rangle$ and $|m'\rangle$ vary in integer steps between $-3/2$ and $+3/2$, are given by the matrix element $|\langle m|I_x|m'\rangle|^2$. In an isotropic liquid the average $\langle R_0^{(2)}\rangle_{\pm}$ is equal to zero thus forcing ν_Q to zero in Eq. (8). Since the three allowed NMR transitions are degenerate in energy, a spectrum with just one peak representing the three overlapping transitions is observed. In filamentous bacteriophage solution the situation is different. Here a spectrum with peaks centered at frequencies $+6\nu_Q$, 0, and $-6\nu_Q$ in a 3/4:1:3/4 intensity ratio is anticipated. The splitting between the $|-3/2\rangle\leftrightarrow|-1/2\rangle$ and the $|+1/2\rangle\leftrightarrow|+3/2\rangle$ satellite transitions is $\Delta\nu = 12\nu_Q$, which provides a direct measure of the average $\langle R_0^{(2)}\rangle_{\pm}$ since β_Q is a constant.

III. CELL MODEL

One way of approximating the average $\langle R_0^{(2)}\rangle_{\pm}$ for $I=3/2$ ions dissolved in bacteriophage solution involves calculation of the potential $V_r(r)$ and the density of positive and negative charges $\rho_{\pm}(r)$ around a filamentous phage particle. The cell model of polyelectrolytes[22] considers one phage particle of length ℓ and radius a as essentially an infinitely long cylinder with q_{rod}/e negative charges smeared uniformly over the surface. Counterions are taken to be freely moving in a medium of permittivity ε and of volume set by the mean distance $2R$ between phage particles. A reasonable starting point in the determination of the potential $V_r(r)$ is the solution to the Poisson equation

$$\nabla^2 V_r(r) = \frac{1}{r}\frac{\partial}{\partial r}\left(r\frac{\partial}{\partial r}V_r(r)\right) = -\frac{\rho(r)}{\varepsilon}, \tag{9}$$

in cylindrical coordinates where $\rho(r)$ is the free charge density that can be written in terms of the potential $V_r(r)$ using Boltzmann statistics as

$$\rho(r) = \rho_+(r) + \rho_-(r) = eN_+e^{-eV_r(r)/kT} - eN_-e^{eV_r(r)/kT}. \tag{10}$$

Although exact analytical solutions to Eq. (9) using Eq. (10) exist with $N_- = 0$ and $N_+ = -q_{\mathrm{rod}}/\mathcal{V}$ where q_{rod} is the negative charge on the Pf1 particle and $\mathcal{V}$ is the volume of the cell, these solutions are not applicable here because in most samples where additional salt is present N_- is nonzero. A combination of high charge on the rod surface, small cell volume, high free charge density, and high dielectric constant $\varepsilon/\varepsilon_0 \approx 80$ rule out application of the Debye–Hückel approximation to Eq. (10). Since the analytic transformation used by Fuoss *et al.*[17] to solve Eq. (9) breaks down with $N_-\neq 0$, the method of relaxation was used to determine numerical solutions for the potential $V_r(r)$ with the boundary conditions of charge neutrality and $dV_r(r)/dr = 0$ at $r=R$. The plots of $V_r(r)$, $\nabla^2 V_r(r)$, $\rho_+(r)$, and $\rho_-(r)$ in Figs. 1(a)–1(d), respectively, show some of the results typical of this numerical calculation. All of the curves in Fig. 1 are appropriate for the same 57 mg/mL electroneutral solution of Pf1 in water with 30 mM added NaCl and $\varepsilon/\varepsilon_0 = 80$. The plot in Fig. 1(a) is consistent with the $2a = 6.6$ nm diameter negative Pf1 rod and the $R = 13$ nm cell radius. The electric potential $V_r(r)$ in Fig. 1(a) is negative at the negative rod surface located at r

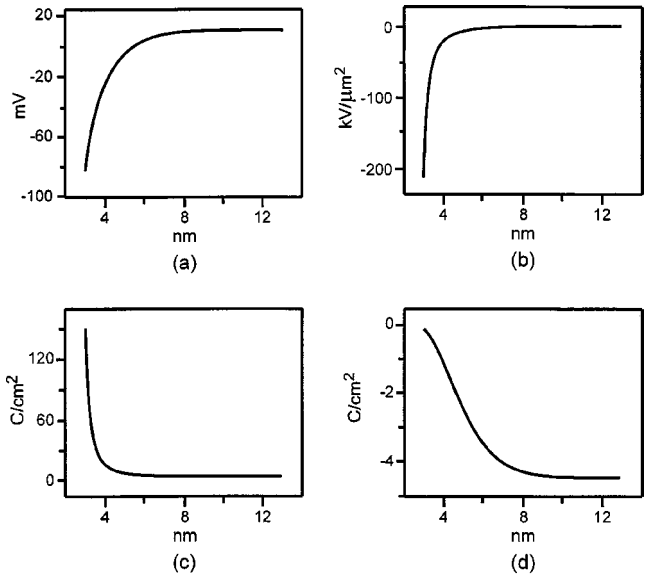

FIG. 1. Numerical solutions to the Poisson equation shown in Eq. (9) for $V_r(r)$, $\nabla^2 V_r(r)$, $\rho+(r)$, and $\rho_-(r)$ in (a)–(d), respectively. All of these curves are appropriate for the same 57 mg/mL electroneutral solution of Pfl in water with 30 mM added NaCl and $\varepsilon/\varepsilon_0=80$.

$=a=3.3$ nm and the condition that $dV_r(r)/dr=0$ at the boundary $r=R$ is maintained. The important parameter for NMR studies is the field gradient $\nabla^2 V_r(r)$ in the region between particles. This gradient is related to the total free charge density by the Poisson equation shown in Eq. (9) and thus the potential $V_r(r)$ in Eq. (10). The result of the calculation of the field gradient $-\rho(r)/\varepsilon$ from the numerical solution for the potential in Fig. 1(a) is shown in Fig. 1(b). As intuitively expected, the regions of nonzero gradient are close to the rod surface while nearly zero values of the gradient are observed for distances of $r>8$ nm from the rod surface. The corresponding positive and negative free charge densities are shown in Figs. 1(c) and 1(d), respectively. Since the positive ion density is largest in the region of nonzero field gradient and the absolute value of the negative ion density is largest far from the rod surface, the absolute value of the average gradient for positive free ions is greater than that for negative free ions. Numerical solutions like those shown in Fig. 1 for different Pf1 concentration and $\varepsilon/\varepsilon_0$, N_+, N_-, and q_{rod} values can be used to generate precise numerical functions for the field gradient $-\rho(r)/\varepsilon$.

The Poisson equation in Eq. (9) can be used to recast the $q=0$ irreducible component of the field gradient tensor in Eq. (5) as

$$R_0^{(2)}(r)=\frac{1-\gamma_\infty}{\sqrt{6}}\frac{\rho(r)}{\varepsilon}, \tag{11}$$

where the definition of $V(r)$ in terms of $V_r(r)$ in Eq. (4) is used. The relationship between the operator $R_0^{(2)}(r)$ and the charge density $\rho(r)$ in the above equation deserves some comment. If one were to directly apply the theory appropriate for field gradient calculations in ionic crystals, then application of a point charge model for the potential at the nucleus would yield $R_0^{(2)}(r)=0$ because each charge would produce a $1/r$ Coulombic potential in accord with LaPlace's

FIG. 2. Summary of ^{23}Na NMR results for a 57 mg/mL Pfl solution including an additional 30 mM of NaCl. The three peak spectrum in (a) results from the application of one rf pulse. The double quantum filtered spectrum shown in (b) is consistent with the simulation shown in (c) using $\nu_Q=167$ Hz and a 60 μs delay time between the termination of the $\pi/2$ rf pulse and the beginning of data acquisition.

equation.[15] However, since the medium involves free charge described here by $\rho(r)$, $R_0^{(2)}(r)$ is nonzero in accord with Poisson's equation shown in Eq. (9).[23] Given the functional form for $R_0^{(2)}(r)$ in Eq. (11) the average $\langle R_0^{(2)}\rangle_\pm$ can be determined from Eqs. (7) and (10) as

$$\langle R_0^{(2)}\rangle_\pm=\frac{\int\rho(r)\rho_\pm(r)rdr}{\sqrt{6}\varepsilon\int\rho_\pm(r)rdr}, \tag{12}$$

where, once again, the charge densities $\rho(r)$ and $\rho_\pm(r)$ are obtained from numerical solutions to Eq. (9).

IV. EXPERIMENT

All NMR spectra for ^{23}Na, ^{79}Br, ^{35}Cl, and ^{39}K at Larmor frequencies of 78.13, 74.06, 28.94, and 13.78 MHz, respectively, were obtained using a homebuilt NMR spectrometer operating at a magnetic field strength of 6.95 T. Filamentous bacteriophage Pf1 was synthesized using the procedure outlined in Ref. 3. Sodium chloride and potassium bromide were obtained from Aldrich chemical company and were used without further purification. All numerical simulations were performed using Fortran code and all data processing,

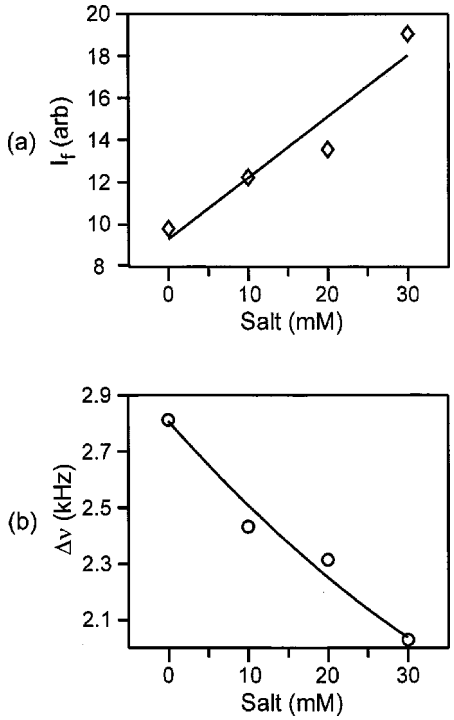

FIG. 3. Summary of ^{23}Na NMR data for the 57 mg/mL Pfl solution as a function of increasing the NaCl concentration of the sample up to 30 mM. The intensity of the triplet center band is shown as diamonds in (a) and increases in a linear fashion with added NaCl as shown by the solid line. The satellite splitting $\Delta\nu$ decreases with added NaCl as shown by the circles in (b). The solid line in (b) corresponds to theory. A conservative estimate of the error in the measurements summarized in (a) and (b) is provided by the size of the data point marker in the plots.

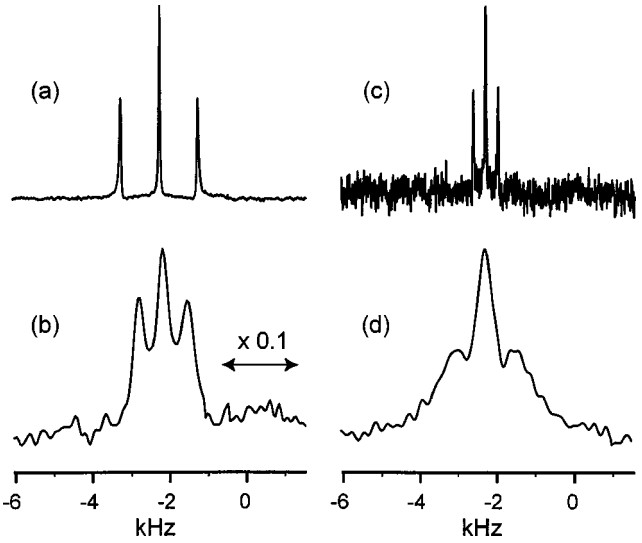

FIG. 4. A survey of monovalent quadrupolar ion NMR spectra in Pfl solution displaying residual quadrupolar couplings for ^{23}Na, ^{35}Cl, ^{39}K, and ^{79}Br nuclei in (a)–(d) respectively. The spectra in (a) and (b) correspond to increasing the NaCl concentration of a 57 mg/mL Pfl solution by 30 mM while the spectra in (c) and (d) correspond to increasing the KBr concentration of a 50 mg/mL Pfl solution by 30 mM.

linear regression, and spectral analysis were accomplished using Matlab. The sum of the differences between electric potentials calculated from Eq. (9) using the method of relaxation at the final time increment was always less than 10^{-9} mV for the potentials used here.

V. RESULTS

The ^{23}Na NMR spectra in Fig. 2 illustrate the spectral consequences of dissolving 30 mM NaCl into a magnetically aligned 57 mg/mL Pf1 solution. The residual Pf1 alignment causes the average $\langle R_0^{(2)}\rangle_\pm$ and hence $\mathcal{H}$ in Eq. (8) to be nonzero. As shown in Fig. 2(a), this produces three equally spaced extremely narrow 41 Hz full width at half maximum (FWHM) resonances centered at -2.2 kHz, the same offset observed for ^{23}Na in a NaCl–water solution. The T_2 for each of these lines was determined to be 26 ms with the spin echo experiment by varying the delay time τ. The spectra shown in Fig. 2(b) correspond to replacement of the π radio frequency (rf) pulse in the spin echo experiment at the time $\tau = 1.42$ ms following the initial $\pi/2$ pulse with a pair of $\pi/2$ pulses phase cycled with the receiver to select signal corresponding to only evolution under $\mathcal{H}$ in Eq. (8). The amplitude and phase of the spectrum in Fig. 2(b) is consistent with the simulation of the double quantum filtered experiment given the 60 μs receiver dead time as shown in Fig. 2(c).

Synthesis of Pf1 bacteriophage involves addition of significant amounts of Na-EDTA. It is most likely, therefore, that the majority of the cations surrounding the polyelectrolyte rod are Na^+. The diamonds in Fig. 3(a) summarize the increase of center peak integrated intensity I_f of the ^{23}Na triplet in Fig. 1(a) as a function of NaCl concentration starting with a sample having no added NaCl and dialyzed to a 30 mM tris-EDTA solution. The background Na^+ ion concentration in the dialyzed sample with no added NaCl is sufficient to observe an NMR signal. The solid line $I_f = (0.29/\text{mM})[Na^+]_{\text{add}} + 9.3$ in Fig. 3(a) corresponds to a linear regression analysis of the measured data. The correlation coefficient for this fit was 0.96. Although the center band of the triplet is used to measure I_f, it is important to note that the satellite integrated intensity also increases by the same amount with added NaCl. The circles in Fig. 3(b) summarize the decrease in the ^{23}Na satellite splitting with added NaCl up to 30 mM. The solid line in this figure corresponds to theory and will be discussed in the next section.

The ion charge sensitive nature of the average $\langle R_0^{(2)}\rangle_\pm$ by aligned Pf1 is displayed in the ^{23}Na, ^{35}Cl, ^{39}K, and ^{79}Br spectra in Figs. 4(a)–4(d), respectively. The ^{23}Na and ^{35}Cl spectra in Figs. 4(a) and 4(b), respectively, correspond to increasing the NaCl concentration of a 57 mg/mL sample of Pf1 dialyzed to 30 mM tris-EDTA by 30 mM. The ^{39}K and ^{79}Br spectra in Figs. 4(c) and 4(d), respectively, correspond to increasing the KBr concentration of a 50 mg/mL sample of Pf1 dialyzed to 30 mM tris-EDTA by 30 mM. The offset frequency of the central peak in each of these spectra is identical to the offset frequency for the free ion dissolved in water. The satellite splitting $\Delta\nu$ for each of these spectra is summarized as a measured quadrupolar coupling constant value $\nu_Q = \Delta\nu/12$ in Table I. The average $\langle R_0^{(2)}\rangle_\pm$ values calculated from the measured ν_Q values and the quadrupole moments Q for each $I = 3/2$ nucleus used in this study are also included in Table I.

TABLE I. Summary of quadrupole coupling parameters.

Ion	Phage (mg/ml)	ν_Q[a] (Hz)	Q ($\times 10^{-29}$ m^2)	$\langle R_0^{(2)}\rangle$ ($\times 10^{17}$ J/Cm^2)
^{23}Na	57	167	1.00	10.2
^{39}K	50	54	0.49	6.7
^{35}Cl	57	11	−1.00	0.7
^{79}Br	50	142	3.70	2.3

[a] $\nu_Q = \Delta\nu/12$ where $\Delta\nu$ is the satellite line splitting.

VI. DISCUSSION

The three sharp lines in the ^{23}Na NMR spectrum in Fig. 1(a) most likely reflect the $|-3/2\rangle \leftrightarrow |-1/2\rangle$, $|-1/2\rangle \leftrightarrow |+1/2\rangle$, and $|+1/2\rangle \leftrightarrow |+3/2\rangle$ transitions for the $I=3/2$ ^{23}Na nucleus in the void space between the phage particles. The splitting of these three peaks is indicative of the Hamiltonian in Eq. (8) because the amplitude and phase of the double quantum filtered spectrum in Fig. 1(b) is consistent with the simulation shown in Fig. 1(c). The simulation shown in Fig. 1(c) was accomplished using density operator methods to analytically solve for the free induction signal following application of the double quantum filtered experiment to an $I=3/2$ nuclear spin with $\nu_Q = 167$ Hz.

Accurate values for the triplet quadrupolar free ion splittings and the amplitude of the three ^{23}Na NMR peaks can be obtained by modeling each line shape as a Gaussian. Figure 3(a) shows the increase in the triplet center band integrated intensity I_f as a function of adding NaCl. The 0.29/mM slope and 9.3 intercept of the solid line for I_f in Fig. 3(a) can be used to determine the background Na^+ ion concentration $[Na^+]_{back}$ before the addition of any NaCl to the phage solution. One basically considers the ^{23}Na NMR signal intensity as the sum of the background and the added sodium ions as $I_f = \eta[Na^+]_{add} + \eta[Na^+]_{back}$ where η is a constant that relates concentration to the measured signal intensity. The slope and intercept of I_f versus $[Na^+]_{add}$ can be used to find $\eta = 0.29$/mM and $[Na^+]_{back} = 9.3/(0.29/\text{mM}) = 32$ mM. This positive ion concentration agrees reasonably well with the anticipated 31.1 mM concentration of negative surface charges in the 57 mg/mL Pf1 solution.

The high surface charge density for Pf1 in solution indicates that the absolute value of the electric potential, field gradient, and positive ion density will be highest near the Pf1 surface as described in Figs. 1(a)–1(c). Concomitantly, any free negative ions will be occluded to the center of the region between particles as shown in Fig. 1(d). The average field gradient in Eq. (12) involves the product of the total charge density $\rho(r)$ with the positive or negative charge density $\rho_\pm(r)$. It is clear from the plots in Figs. 1(b)–1(d) that the product $\rho(r)\rho_+(r)$ for positive ions will extract larger gradient values than the corresponding product $\rho(r)\rho_-(r)$ for negative ions. The integral over the positive product will therefore be larger than the corresponding integral over the negative product. Hence, positive ions in Pf1 solution should display larger average field gradient values than negative ions. It is clear from Figs. 4(a) and 4(b) that the splitting $\Delta\nu$ for ^{23}Na is at least an order of magnitude larger than that for ^{35}Cl. This comparison is straightforward since the quadrupole moments for ^{23}Na and ^{35}Cl are of opposite sign but the same size. A similar visual comparison for ^{39}K and ^{79}Br in Figs. 4(c) and 4(d), respectively, is less revealing. Here the quadrupole moments for ^{39}K and ^{79}Br differ by almost an order of magnitude as shown in Table I. In this case the best comparison of charge effects in Pf1 solution is to instead calculate the average $\langle R_0^{(2)}\rangle_\pm$ from the splitting $\Delta\nu$, ν_Q, and β_Q values as shown in Table I. The first two rows of Table I show the average $\langle R_0^{(2)}\rangle_+$ as determined from Figs. 4(a) and 4(c) respectively, while the last two rows show the average $\langle R_0^{(2)}\rangle_-$ as calculated from Figs. 4(b) and 4(d), respectively. It is clear from Table I that the average $\langle R_0^{(2)}\rangle_+ = 10.2$ and 6.7 values for positive ions is larger than the $\langle R_0^{(2)}\rangle_- = 0.7$ and 2.3 values for negative ions. This comparison is much more severe when the effects of the field gradient on the valence electrons of the ion embodied by the Sternheimer antishielding factor are included. Unfortunately these factors are only available for ionic crystals, not ions in aqueous fluid phase experiencing a gradient $-\rho(r)/\varepsilon$. One would expect upon going from the case of the ionic crystal to that of the aqueous ion, the value for the antishielding factor would change but the trend with the number of valence electrons would remain largely constant. Indeed the Sternheimer factors appropriate for ionic crystals involving the two negative ions examined here are much larger than those for the positive ions. Given that the ionic crystal values[24] predict a ^{35}Cl–^{23}Na ratio of 57.6/5.1=11.3 and a ^{79}Br–^{39}K ratio of 101/18.3=5.5, one would anticipate that the expected average $\langle R_0^{(2)}\rangle$ values reported in Table I would slightly magnify the effects of the Pf1 induced field gradient on the free positive ions and greatly magnify the same effect on the free negative ions. The net consequence of these factors is to greatly emphasize the effect of the field gradient on the negative ion and thus make the average $\langle R_0^{(2)}\rangle_-$ values anomalously closer to the average $\langle R_0^{(2)}\rangle_+$ values in Table I.

Although the trends in Fig. 4 and Table I agree with the solution of the Poisson–Boltzmann equation, the accuracy of the approach in the description of residual quadrupolar effects must be addressed. A good comparison between theory and experiment is shown in Fig. 3(b). The circles correspond to experimental measurement of the ^{23}Na satellite splitting $\Delta\nu$ as a function of added NaCl. The solid line in Fig. 3(b) corresponds to the value of the average $\langle R_0^{(2)}\rangle_+$ calculated from Eq. (12) and the numerical solution for $V_r(r)$ from Eq. (9). The calculation assumes that the Pf1 alignment is saturated along the direction of the magnetic field and that a 57 mg/mL rod concentration, a dielectric constant of $\varepsilon/\varepsilon_0 = 80$ appropriate for water, an electron charge of $e = 1.6 \times 10^{-19}$ C, a Boltzmann's constant of $k = 1.38 \times 10^{-23}$ J/K, a temperature of $T = 298$ K, and a variable added ion concentration from 0 to 30 mM are present. In order to make the theoretical curve agree with the experimental data a Sternheimer factor of 13.3 was used. Even though the Sternheimer factor used here is roughly a factor of two greater than the 5.1 ionic crystal value,[24] the agreement between experiment and theory in Fig. 3(b) is remarkable. The potential $V_r(r)$ for the 30 mM free ion concentration can be used to calculate the $\Delta\nu = 132$ Hz ^{35}Cl residual quadrupolar

splitting. Good agreement between experiment and theory is obtained with a Sternheimer factor of 109.5, again a value roughly a factor of 2 greater than anticipated from ionic crystal values.[24] Similar calculations of $\Delta\nu$ values for the ^{39}K and ^{79}Br isotopes also produce discrepancies between ionic crystal and aqueous phase Sternheimer factors. It is clear that the accuracy of the comparison of experimental data with theory is limited by the lack of Sternheimer antishielding factors for ions in partially ordered phase. Given the current high precision and availability of basis functions for the atomic ions considered here combined with the numerical values of the potential $V_r(r)$, one could in principle evaluate the necessary Sternheimer factors. The size and nature of such an endeavor deserves its own venue and is beyond the scope of the present work. It is, however, pleasing that the relative size of the Sternheimer factors deduced from the comparison of experiment with theory for the ^{23}Na and ^{35}Cl ions largely agree with ionic crystal values.

Finally, it is important to compare the cell model of polyelectrolytes employed here to explain the recovery of residual quadrupolar couplings with other theoretical models typically used to understand electrochemical boundary layer phenomena. This theory is admittedly of the Gouy–Chapman family since a diffuse free ion layer is naturally included and the surface ion binding indicative of both the Helmholtz and Stern models of electrolyte solutions is neglected.[25] The neglect of the Stern layer in the cell model is justified here by comparison of the 32.1 mM free ^{23}Na ion concentration with the anticipated 31.1 mM surface charge in a 57 mg/mL Pf1 solution. This comparison suggests a complete absence of tightly bound positive surface ions. The cell model does differ from the standard Gouy–Chapman approach in the choice of boundary conditions. Gouy–Chapman theory assumes that both $dV_r(r)/dr=0$ and $V_r(r)=0$ at $r=\infty$ and that the electrolytic solution is charge neutral with respect to itself. The cell model on the other hand incorporates the charge of the cell boundary and the cell dimensions into its boundary conditions as mentioned above.

VII. CONCLUSION

The NMR spectra of $I>1/2$ quadrupolar nuclei provide a very sensitive probe of anisotropic organized materials. A model based on a solution to the Poisson–Boltzmann equation for the recovery of quadrupolar couplings in filamentous bacteriophage solution for positive and negative ions was developed and compared to experiment. The agreement between experiment and theory is remarkable even in the absence of reasonable estimates of Sternhemier antishielding factors for ions in aqueous liquid phase. The first step towards further refining the theoretical model includes the estimation of Sternheimer factors due to the gradient $-\rho(r)/\varepsilon$. Further examination of the splitting $\Delta\nu$ as a function of both temperature and magnetic field will be helpful in improving the crude theory presented here. The effect of temperature will be to change both the alignment of the Pf1 particles via the average over the angular function $d^{(2)}_{q,0}(\beta)$ in Eq. (6) and the ion distribution around the Pf1 particles shown in Eq. (10). Satellite splittings as a function of magnetic field will reveal the dependence of the average $\langle R^{(2)}_0\rangle_{\pm}$ on the alignment of the Pf1 particles via the average over the angular function $d^{(2)}_{q,0}(\beta)$ in Eq. (6). Finally, future NMR and optical experiments involving multivalent main group and lanthanide ions will lead to a wide range of experimental data useful for comparison of experiment with theory.

ACKNOWLEDGMENTS

The authors are indebted to both Susan Tucker and Paul Feldstein for useful conversations and aid in sample preparation. Support from the NSF under Grant No. CHE-9984654 is gratefully acknowledged. M.P.A. is a David and Lucile Packard Foundation and Alfred P. Sloan Foundation fellow.

[1] N. Tjandra and A. Bax, Science **278**, 1111 (1997).
[2] G. M. Clore, M. R. Starich, and A. M. Gronenborn, J. Am. Chem. Soc. **120**, 10571 (1998).
[3] M. R. Hansen, L. Mueller, and A. Pardi, Nat. Struct. Biol. **5**, 1065 (1998).
[4] R. R. Ernst, B. Bodenhausen, and A. Wokaun, *Principles of Nuclear Magnetic Resonance in One and Two Dimensions* (Oxford, New York, 1997).
[5] J. W. Emsley and J. C. Lindon, *NMR Spectroscopy Using Liquid Crystal Solvents* (Pergamon, New York, 1975).
[6] G. N. Patey, E. E. Burnell, J. G. Snijders, and C. A. de Lange, Chem. Phys. Lett. **99**, 271 (1983).
[7] H. Wennerström, B. Lindman, S. Engström, G. Lindblom, and G. J. T. Tiddy, in *Magnetic Resonance in Colloid and Interface Science*, edited by J. P. Fraissard and H. A. Resing (Reidel, Boston, 1980), p. 609.
[8] J. G. Snijders, C. A. de Lange, and E. E. Burnell, J. Chem. Phys. **77**, 5386 (1982).
[9] L. W. Reeves and A. S. Tracey, J. Am. Chem. Soc. **96**, 365 (1974).
[10] J. Charvolin, A. Lowenstein, and J. Virlet, J. Magn. Reson. **26**, 529 (1977).
[11] G. Lindblom, H. Wennerström, and B. Lindman, in *Magnetic Resonance in Colloid and Interface Science*, edited by H. A. Resing and C. G. Wade (ACS Symposium Series, American Chemical Society, Washington, DC, 1976), p. 372.
[12] H. Wennerström, B. Lindman, G. Lindblom, and G. J. T. Tiddy, J. Chem. Soc. Faraday Trans. **75**, 663 (1979).
[13] H. Wennerström, G. Lindblom, and B. Lindman, Chem. Scr. **6**, 97 (1974).
[14] R. M. Sternheimer and R. F. Peierls, Phys. Rev. A **3**, 837 (1971).
[15] M. H. Cohen and F. Reif, Solid State Phys. **5**, 321 (1957).
[16] J. J. Van der Klink, L. H. Zuiderweg, and J. C. Leyte, **60**, 2391 (1974).
[17] R. M. Fuoss, A. Katchalsky, and S. Lifson, Proc. Natl. Acad. Sci. U.S.A. **37**, 579 (1951).
[18] K. Zimmermann, H. Hagedorn, C. C. Heuck, M. Hinrichsen, and H. Ludwig, J. Biol. Chem. **261**, 1653 (1986).
[19] M. H. Cohen, Ph.D. thesis, University of California, Berkeley, 1952.
[20] R. M. Sternheimer and H. M. Foley, Phys. Rev. **102**, 731 (1956).
[21] T. P. Das and R. Bersohn, Phys. Rev. **102**, 733 (1956).
[22] A. Katchalsky, Z. Alexandrowicz, and O. Kedem, in *Chemical Physics of Ionic Solutions*, edited by B. E. Conway and R. G. Barradas (Wiley, New York, 1966), p. 302.
[23] C. P. Slichter, *Principles of Magnetic Resonance* (Springer-Verlag, New York, 1990).
[24] E. A. C. Lucken, *Nuclear Quadrupole Coupling Constants* (Academic, New York, 1969).
[25] M. J. Sparnaay, The Electrical Double Layer, in *The International Encyclopedia of Physical Chemistry and Chemical Physics*, edited by D. D. Eley and F. C. Tompkins (Pergamon, New York, 1972), p. 57.